Contributions to Mineralogy and Petrology (2024) 179:41
https://doi.org/10.1007/s00410-024-02127-y

ORIGINAL PAPER

Experimental re-melting of a continental crust: probing the deep storage zone of Campi Flegrei and Vesuvius magmas

Flavia Palummo[1] · Cristina Perinelli[1] · Barbara Bonechi[2] · Alessandro Fabbrizio[3] · Valeria Misiti[4] · Piergiorgio Scarlato[4] · Mario Gaeta[1]

Received: 15 November 2023 / Accepted: 22 March 2024

Abstract
Mantle magmas interact with surrounding rocks during their ascent and storage in the continental crust, leading to open system processes as wall rock partial melting. In this study, we have experimentally investigated the reactions between a leucosome depleted migmatite and a primitive K-basaltic of Campi Flegrei (Italy). Experiments were carried out at pressure of 0.8 GPa temperatures from 1250 °C to 1050 °C and constant temperature and thermal gradient conditions. The experimental products consist of biotite-free migmatite, glass and crystals of clinopyroxene, olivine, plagioclase and Cr-spinel with proportions that vary as a function of temperature. Open system isothermal experiments indicate that the chemistry of melts and phase relationships are controlled by the high Al_2O_3 content of leucosome depleted migmatite with the glass composition shifting from K-trachybasalt towards shoshonite as the temperature decreases from 1200 °C to 1125 °C. At temperatures $\leq$ 1150°C, migmatite assimilation is not exclusively due to the assimilation fractional crystallization process because evidence of mingling and mixing is observed. T-gradient experiment shows melt composition ranging from shoshonite to phono-tephrite moving from the slightly crystalline zone (T = 1250–1210 °C) at the bottom of the capsule towards the highly crystalline zone (T = 1160–1140 °C). This SiO_2-constant trend indicates that at temperature below the basalt solidus, the assimilation of leucosome depleted crust is represented almost exclusively by the biotite breakdown, leading to the increase in Al, Mg, Fe, Ti, and K activities in the system. The shoshonitic composition obtained in our experiments could represent the parental magma for both Campi Flegrei volcanic district and Vesuvius magmatic systems, indicating modification in a deep storage zone through mixing with the partial melts derived from restitic continental crust.

Keywords Magma-crust interaction · Partial melting · Assimilation process · Differentiation processes · K-alkaline basalt · Migmatite

Introduction

During ascent toward the upper continental crust, primitive basaltic magma has the potential to interact with surrounding rocks (Gaeta et al. 2009; Di Rocco et al. 2012; McLeod et al. 2012; Borisova et al. 2021; Knuever et al. 2023; Dallai et al. 2022). Heat released from the mafic magmas induces partial melting of the wall rocks and mineral dissolution (Bowen 1928; Sinigoi et al. 1995; Perinelli et al. 2008; Borisova et al. 2021), so that mantle-derived melts experience distinct lines of descent, resulting into different magmas (Sinigoi et al. 1995). Magma-rock interactions and the resulting magma assimilation (De Paolo 1981) and as well as magma mixing and magma degassing processes regulate composition, volatile content, physical-chemical

Communicated by Othmar Müntener.

✉ Cristina Perinelli
cristina.perinelli@uniroma1.it

[1] Dipartimento di Scienze della Terra, Sapienza Università di Roma, P. le Aldo Moro 5, Rome 00185, Italy

[2] Department of Earth and Environmental Sciences, The University of Manchester, Manchester M13 9PL, UK

[3] Dipartimento di Scienze dell'Ambiente e della Terra, Università Milano-Bicocca, Piazza della Scienza 4, Milan 20126, Italy

[4] Istituto Nazionale di Geofisica e Vulcanologia, Sezione di Roma 1, Via di Vigna Murata 605, Rome 00143, Italy

Published online: 09 April 2024

properties and mobility of melt (Borisova et al. 2021). However, different factors (e.g., pressure, fO_2, magma and wall-rock compositions, volatile content in melt) provide a fundamental control on the efficiency of magma-rock interaction (Borisova et al. 2021). The degree to which mantle and crustal reservoirs have contributed to the geochemical signatures of volcanic rocks is frequently assessed through combined assimilation and fractional crystallization models (Spera and Bohrson 2001; McLeod et al. 2012). The assimilation component is generally represented by partial melts derived from a fertile (i.e., not melted) continental crust in spite that multiple melting episodes are the rule, rather than the exception, in many orogenic zones. This scenario is of primary interest, for example, in the peri-Tyrrhenian orogenic zone where, the emplacement of anatectic crustal magmas, predates the mantle derived volcanism (Peccerillo 2017). The manuscript focuses on the direct investigation (i.e., high pressure and high temperature experiments) of AFC processes during the magma storage in the deep continental crust not just on the differentiation of ascending mantle-derived magmas.

Experimental and analytical methods

Experimental strategy

To investigate the magma-lower crust interaction during the continuous basaltic underplating at the crust-mantle boundary, we have conceived three experimental conditions: (i) closed- and (ii) open-systems at constant temperature, and (iii) open-system with a thermal gradient. Experiments were carried out at pressure of 0.8 GPa, corresponding approximately to the crustal-mantle boundary in the Tyrrhenian Sea region (Peccerillo 2017). A primitive alkaline basalt was used as mantle-derived magma, while a leucosome depleted migmatite was chosen as analogous of the lower continental crust.

Constant temperature experiments were conducted to evaluate the solidus and liquidus temperature of the migmatite and to investigate the assimilation fractional crystallization process (hereafter AFC) at temperatures higher than 1000 °C corresponding to the K-basalt solidus. These temperature conditions ensure the presence of analysable glasses in the capsule, nevertheless, large amount of migmatite melting is predictable (Vielzeuf and Schmidt 2001). The presence of the thermal gradient in the open-system experiment is fundamental to prevent total melting of the crustal rock, despite the experiment was carried out at the hot spot temperature of 1250 °C to remain under the liquidus temperature of the K-basalt. The proposed experimental strategy allows us to simulate the AFC process at temperatures ranging from the solidus to the liquidus of migmatitic rocks and to compare phase relationships and compositions of the basaltic system obtained in open- and closed-system conditions, respectively (Perinelli et al. 2019).

Table 1 Composition (wt%) of APR16 and CT54B starting materials

Sample	APR16*	CT54B‡
Mineral phases¥	Ol, Cpx	Qz, Kfs, Plg, Bt, Crd, Mag, Ilm, Hc, Crn
SiO_2	48.89	58.04
TiO_2	1.23	0.82
Al_2O_3	15.65	19.00
FeO	8.08	7.13
MnO	0.14	0.07
MgO	8.89	3.43
CaO	11.64	1.10
Na_2O	2.88	2.01
K_2O	1.52	5.03
P_2O_5	0.31	0.10
Total	99.23	96.73
L.O.I.	0.61	2.37

¥Phenocrysts/minerals of natural K-basaltic clast/migmatite : Ol olivine; Cpx clinopyroxene; Qz, quartz; Kfs, K-feldspar; Plg, plagioclase; Bt, biotite; Crd, cordierite; Crn, corundum; Hc, hercynite; Mag, magnetite; Ilm, ilmenite

*APR16 composition from Perinelli et al. (2019)

‡CT54B composition from Gaeta et al. (2018)

Starting materials

The basaltic starting material is a natural rock powder obtained from a primitive K-basaltic scoria clast (APR16 sample; Table 1) included in the deposits of Solchiaro hydromagmatic eruption (between 19 ± 6 ka and 14 ± 3 ka; Morabito et al. 2014) located in Procida Island (Campi Flegrei, Italy). The APR16 sample (Mg# = 0.66, $\Sigma_{alkalis}$ = 4.4 wt%) consists of 12 vol% of olivine (Ol), clinopyroxene (Cpx), plagioclase (Plg), Ti-magnetite, potassium feldspar (K-feld) and glass (Mazzeo et al. 2014). The powder used as starting material was obtained by grinding the APR16 rock sample in an agate mortar under acetone.

The starting material analogous of the lower continental crust is a migmatite (CT54B sample; Table 1) belonging to the Gennargentu Igneous Complex (Sardinia, Italy). The migmatite is a leucosome depleted diatexite characterized by fine grained ($\leq$ 200 µm), granoblastic and foliated texture, and hosts a mineral assemblage of quartz (Qtz), K-feld, Plg, biotite, cordierite, ilmenite, hercynite and corundum (Crn; see Gaeta et al. 2018 for further details). CT54B sample was cut in small parallelepiped shapes (~2 × 2 × 3 mm) at the Rock and Thin Section Laboratory of the Department of Earth Sciences of Sapienza University of Rome.

Experimental procedure and capsule preparation

Experiments were performed by using two types of piston cylinder, the 1 inch non-end loaded piston cylinder apparatus (QUICKpress type, Depths of the Earth co.) at the HP-HT Laboratory of Experimental Volcanology and Geophysics of Istituto Nazionale di Geofisica e Vulcanologia (Roma, Italy) for the thermal gradient experiment, and the ½ inch end-loaded piston cylinder apparatus at the HP-HT Laboratory of the Department of Earth Sciences of Sapienza University of Rome for constant temperature experiments. Experiments were carried out at the isobaric pressure of 0.8 GPa, dwell times of 1–2 h and in the temperature range of 1250–1050 °C (see Table 2 for details), under natural water conditions. Temperature conditions were chosen on the basis of crystallization degree and phase equilibria of experimental runs from Perinelli et al. (2019) and Bonechi et al. (2020) and has to be lower than the liquidus temperature of the basalt (i.e., 1280 °C for the APR16 sample at 0.8 GPa, as reported in Perinelli et al. 2019). The assembly for constant temperature experiments consists of an outer CaF_2 cell, graphite furnace and MgO crushable spacers, while for thermal gradient experiment a NaCl-Pyrex-graphite-crushable MgO assembly was used. The $Au_{75}Pd_{25}$ capsule was placed in the MgO crushable spacers and surrounded by powder of alumina.

Two sets of closed system experiments were performed, filling 6-mm long capsules with basaltic powder (APR16 sample) and migmatite powder (CT54B sample), respectively. The open-system conditions were studied with two experimental sets (thereafter constant temperature and T-gradient experiments). Constant temperature experiments were performed using parallelepiped pieces of migmatite placed in the upper part of the capsule and surrounded by basaltic powder of APR16 (Fig. 1a). Instead, the set-up of the capsule for the T-gradient experiment was made packing the bottom of the capsule with a layer of powdered APR16 (59.8 mg), on which the parallelepiped shape migmatite (15.6 mg) was placed (Fig. 1b). Constant temperature experiments were performed using 6-mm long capsules, in order to maintain the sample in the furnace hot spot. T-gradient experiment was designed taking advantage of the innate temperature gradient of the piston cylinder apparatus (Masotta et al. 2012 and references therein). This experiment

Table 2 Experimental run conditions, phases assemblage and proportions (vol%) in run products

Run #	Capsule zone	T (°C)	H_2O_i * (wt%)	Time (h)	Gl	Cpx	Ol	Plg	Ox	Crystallization degree (vol%)
Closed system experiments‡										
APR16-14		1310	0.61	1	100					
APR16-11		1290	0.61	3	100					
APR16-26		1270	0.61	3	100	trace				<<1
APR16-12		1250	0.61	3.3	91	9				9
APR16-35		1225	0.61	6	89	11				11
APR16-24		1190	0.61	9	74	22	1	3	trace	26
APR16-GLAd		1250	0.61	3	83	16	1		trace	17
APR16-GLAb		1220	0.61	6	63	26	2	9	1	37
APR16-GLBd1		1200	0.61	9	55	31	2	11	1	45
APR16-GLBd2		1170	0.61	9	50	32	3	14	1	50
SCE-9		1295	0.61	3	100	trace				<<1
SCE-11		1270	0.61	3	76	19	4			24
SCE-12		1235	0.61	6	65	26	5	2	2	35
CT54M_1		1050	2.37	1	65					35
Open system experiment										
APR16_M_GRAD	*Zone 1*	1250 – 1210	0.95	1	65	24	3	6	2	35
	Zone 2	1210 – 1180		1	60	27	2	10	1	40
	Zone 3	1180 – 1160		1	45	27	5	20	2	55
	Zone 4	1160 – 1140		1	40	28	6	24	2	60
	Zone 5	1140 – 1000		1	0	39	11	46	4	100
APR16_M2	*top zone*	1200	0.95	1	73	25	2		trace	27
	bottom zone	1200		1	51	28	6	13	2	49
APR16_M4		1200	0.95	2	75	21	2		2	25
APR16_M3	*basaltic zone*	1150	0.95	1	47	26	7	19	1	53
APR16_M5	*basaltic zone*	1125	0.95	1	41	32	7	18	2	59

* $H2O_i$ is nominal content (wt%) of water in the charge calculated assuming all L.O.I. of APR16 and CT54M rocks as H_2O; Gl = glass; Cpx = clinopyroxene; Ol = Olivine; Plg = plagioclase; Ox = oxide minerals

‡ Closed system experiments data are from Perinelli et al. (2019)

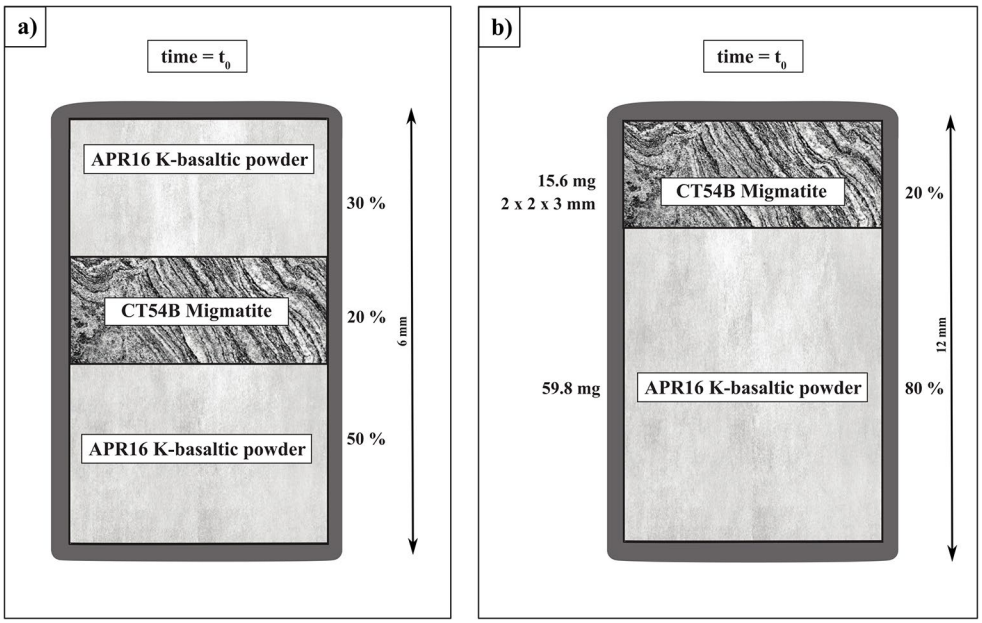

Fig. 1 Scheme of the starting configuration of the two types of experiment described: (a) isothermal experiments performed using parallelepiped pieces of migmatite (20 wt%) placed in the upper part of the 6-mm long capsule and surrounded by basaltic powder of APR16 (80 wt%); (b) T-gradient experiment established packing the bottom of the 12-mm long capsule with a layer of powdered APR16 (80 wt%), on which the parallelepiped shaped migmatite (20 wt%) was positioned

was carried out by using a longer capsule (12 mm), in order to have the top of the capsule a few millimetres above the furnace hot spot zone. Temperature was measured using a C-type W_5Re_{95}-$W_{26}Re_{74}$ thermocouple and manually controlled within an uncertainty of ± 5 °C.

Analytical methods

The recovered samples have been mounted in epoxy resin, ground flat and polished for microanalyses. Textures and phase assemblages were analysed through the acquisition of backscattered electron (BSE) images, using a FEI Quanta-400 scanning electron microscope (SEM) equipped with an EDAX Genesis microanalysis device available at the Department of Earth Sciences of Sapienza University of Rome.

Major element mineral and glass compositions were analysed with an electron probe microanalyzer (EPMA) field emission gun (FEG) electron source JXA-8530 F by Jeol, equipped by 5 wave dispersive spectrometers (WDS) allowing quantitative microanalysis of elements in range from Be to U, installed at the Institute of Petrology and Structural Geology, Charles University of Prague (Prague, Czech Republic). Data were collected by setting 15 kV accelerating voltage and 10 nA electric current. The beam size was 10 µm, with a counting time of 20 s for all elements, except for Na, K, and S, for which counting times of 10 s (Na and K) and 30 s (S) were employed respectively. Standards for calibration were quartz (Si), corundum (Al), rutile (Ti), magnetite (Fe), periclase (Mg), rhodonite (Mn), albite (Na), sanidine (K), diopside (Ca), apatite (P and F), tugtupite (Cl) and anhydrite (S).

Crystal fractions and phase proportions were calculated using bulk and experimental phase compositions, and the least squares regression routine implemented in the EXCEL® program. Image analyses conducted with ImageJ® (Abramoff et al. 2004) software also shows a good correspondence with mass balance results.

In order to constrain temperatures along the furnace, the thermal gradient determined for the assembly during the experiment was then compared with geothermometric calculations (see Supplementary materials for further details).

Closed-system experiments

K-basalt composition

Results of phase equilibria experiments at pressure of 0.8 GPa using K-basalt compositions are described by Perinelli et al. (2019). Here we report the main aspects of experiments performed under nominal water conditions comparable with those of open system experiments.

All the experimental products consist either of glass or glass coexisting with crystal phases (Table 2). Cpx is the liquidus phase (1295–1270 °C) and, according to Morimoto et al. (1988) classification, its composition changes from diopside to augite ($Wo_{43-50}En_{41-49}Fs_{8-9}$) decreasing run temperature. Ol (Fo_{85-88}) and Cr-spinel crystallize at 1250 °C, while Plg, whose composition shifts from bytownitic (An_{70-76}) to labradoritic (An_{59-61}) with the decrease of experimental temperatures, joins the phase assemblage at 1235–1190 °C. Note that the crystallization reaches values of ~ 30 wt% at the lower temperature of 1190 °C (Fig. 2).

Composition of experimental glasses plotted in the total alkali versus silica classification diagram (TAS; Le Maitre et

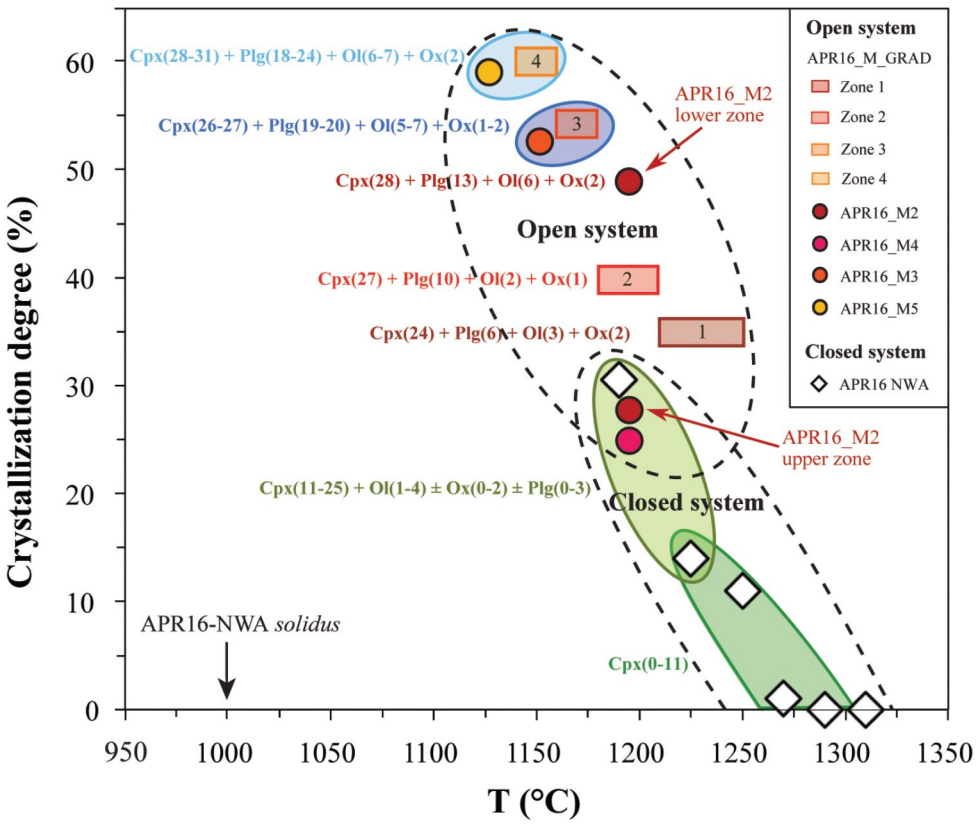

Fig. 2 Solid fraction (by weight) as a function of temperature for isothermal and T-gradient experiments in open system and for phase equilibria experiments in closed system at pressure of 0.8 GPa using K-basalt as starting material under natural water conditions. Modified from Perinelli et al. (2019). Point 1: upper zone of the capsule; point 2: bottom zone of the capsule. NWA: no water addition to the starting materials

al. 2002) varies from K-basalt to K-trachybasalt up to shoshonite with decreasing temperature (Fig. 3). In particular, before reaching the temperature at which Plg significantly crystallizes, the glass composition is controlled by Cpx crystallization thus leading to a very limited SiO_2 increase in the residual glasses (from ~49 to ~50 wt%; Figs. 3 and 4). Moreover, the dominant crystallization of Cpx drives to a decrease of CaO contents (from ~12.1 to ~9.8 wt%) and to an increase of Al_2O_3 contents (from ~15.5 to ~18 wt%) until Plg crystallizes (Fig. 4).

Migmatitic composition

Closed system experiment conducted at 0.8 GPa and 1050 °C using as starting material the powdered migmatite (CT54B in Table 1) results in ~65 wt% of partial melting and the presence of Qtz, Plg ($An_{50–52}$), enstatitic orthopyroxene ($Wo_{0-1}En_{58-68}Fs_{32–42}$), biotite with variable TiO_2 contents (1.6–4.3 wt%), apatite and hercynites to titanomagnetites oxides (Table S1).

Qtz is anhedral and scattered according to its restitic origin analogous to the rare residual crystals of biotite (Fig. 5a). The other mineral phases, including the new hypidiomorphic mica platelets, are euhedral with sizes up to ~10 µm and clustered according to a solid solution recrystallization during the partial melting process.

The composition of glass is characterized by high contents of SiO_2 (~68.8 wt%), alkali (~9 wt%) and Al_2O_3 (~17.2 wt%), coupled with low values of MgO (from ~1 wt%) and CaO (~1 wt%; Table S2). The glass is granitic (normative $Qtz_{30}Or_{50}Alb_{16}An_4$), peraluminous (normative Crn_5) and plot close to the Qtz-Or cotectic of the haplogranitic system at P_{H2O} = 1 GPa (Fig. S1; Couch et al. 2003).

Open-system experiments

Constant temperature experiments

Open system experiments conducted at constant temperatures (Table 2) show that migmatite is completely melted at a temperature of 1200 °C, while several restitic oxide crystals are achieved at 1150 °C and 1125 °C; thus, the liquidus temperature of the migmatite must be slightly above 1150 °C, in agreement with conditions predicted by MELTS (Ghiorso and Sack, 1995; Asimow and Ghiorso, 1998).

In the run conducted at 1200 °C with a dwell time of 1 h, three distinct zones can be identified: (1) in the upper part of the capsule (hereafter *top zone*; Fig. 5b and Fig. S2), the melted migmatite is characterized by the recrystallization of small, clustered hercynitic oxides that join together to form larger crystals. (2) As shown in Fig. 5b, surrounding the melted migmatite there is an area (crystal fraction = ~27

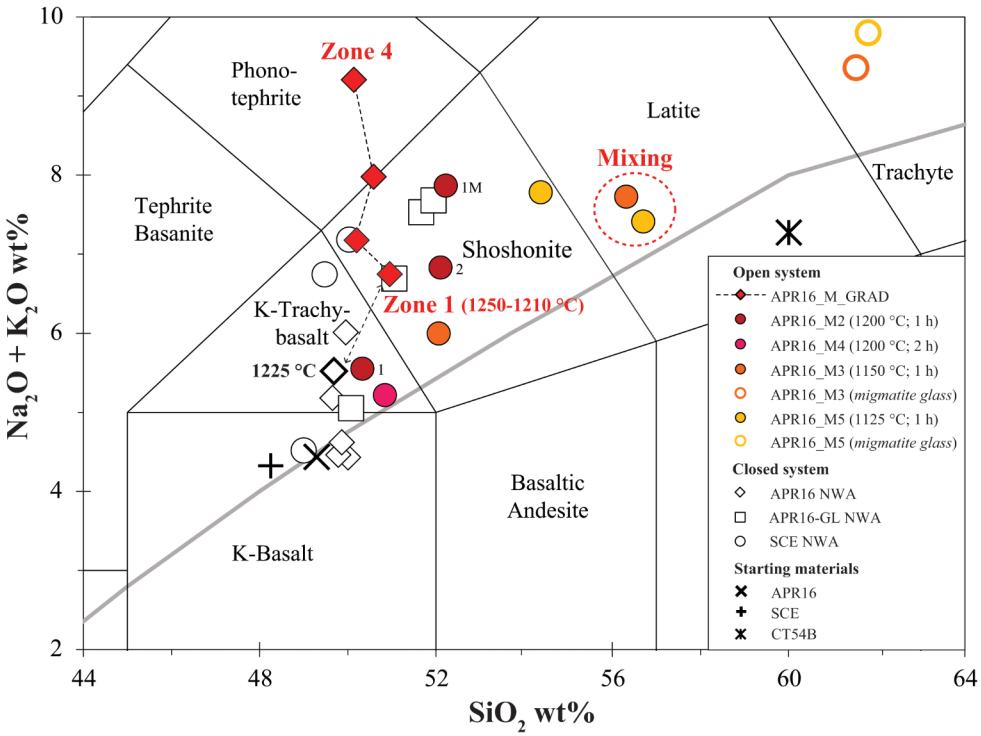

Fig. 3 Total alkali ($Na_2O + K_2O$) vs. silica (SiO_2) diagram (TAS; Le Maitre et al. 2002), illustrating the composition of experimental glasses. Residual glasses of isothermal runs in open system cover the range of K-trachybasalt, shoshonite, latite and trachyte, those of T-gradient run in open system fall in the shoshonite and phono-tephrite fields, whereas those of phase equilibria experiments in closed system are K-basaltic, K-trachybasaltic and shoshonitic in composition. Alkaline/subalkaline limit (grey line) is after Irvine and Baragar (1971). Point 1: upper zone of the capsule; point 2: bottom zone of the capsule; point 1 M: migmatite zone of the capsule. capsule. Details on the petrography and composition of SCE K-basaltic sample are in Bonechi et al. (2020). NWA: no water addition to the starting materials

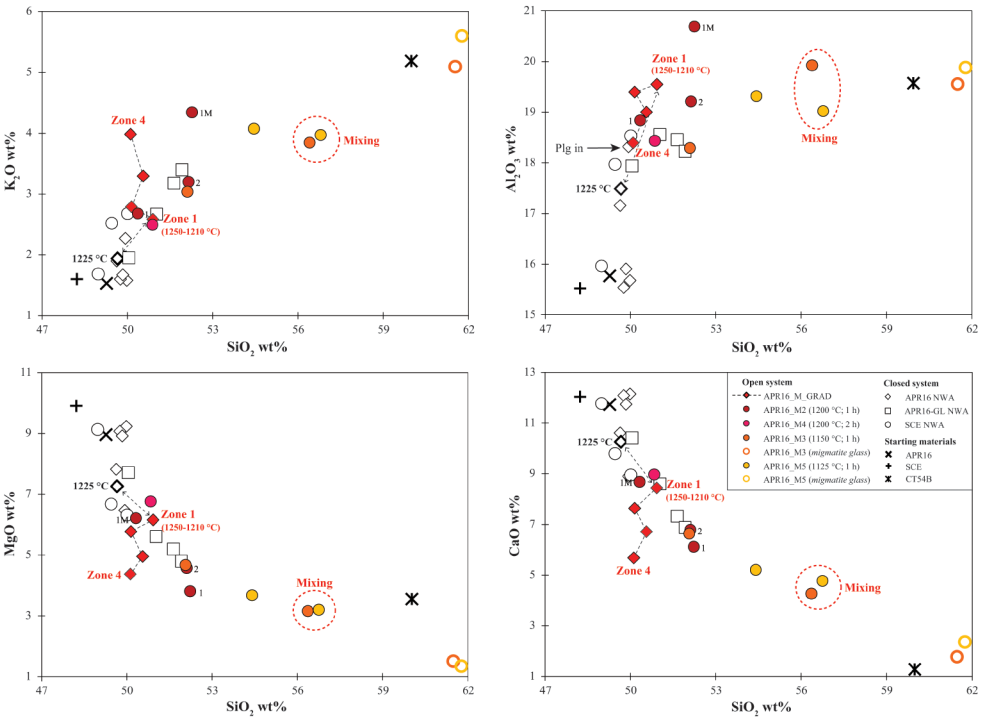

Fig. 4 K_2O, Al_2O_3, MgO and CaO oxides of the experimental glasses plotted versus SiO_2 contents for isothermal and T-gradient experiments in open system and for phase equilibria experiments in closed system. Point 1: upper zone of the capsule; point 2: bottom zone of the capsule; point 1 M: migmatite zone of the capsule

vol%) where Cpx, occasionally zoned diopside core to augite rim ($Wo_{41-49}En_{42-49}Fs_{10-11}$), occurs as the dominant phase (~25 vol%), along with forsteritic Ol (Fo_{83-86}; ~2 vol%) and Al-rich chromite oxides (<1 vol%; Fig. 2; Table 2). (3) In the *bottom zone* of the capsule (Fig. 5c; Fig. S2) the crystal fraction reaches values up to ~49 vol% (Fig. 2; Table 2) with a higher amount of diopsidic Cpx ($Wo_{48-49}En_{41}$-Fs_{10-11}; ~28 vol%), bytownitic Plg (An_{71-75}; ~13 vol%), Ol (Fo_{86-87}; ~6 vol%) and Al-rich chromites (~2 vol%).

In the run conducted at 1200 °C with a dwell time of 2 h, migmatite in the inner portion of the capsule is totally

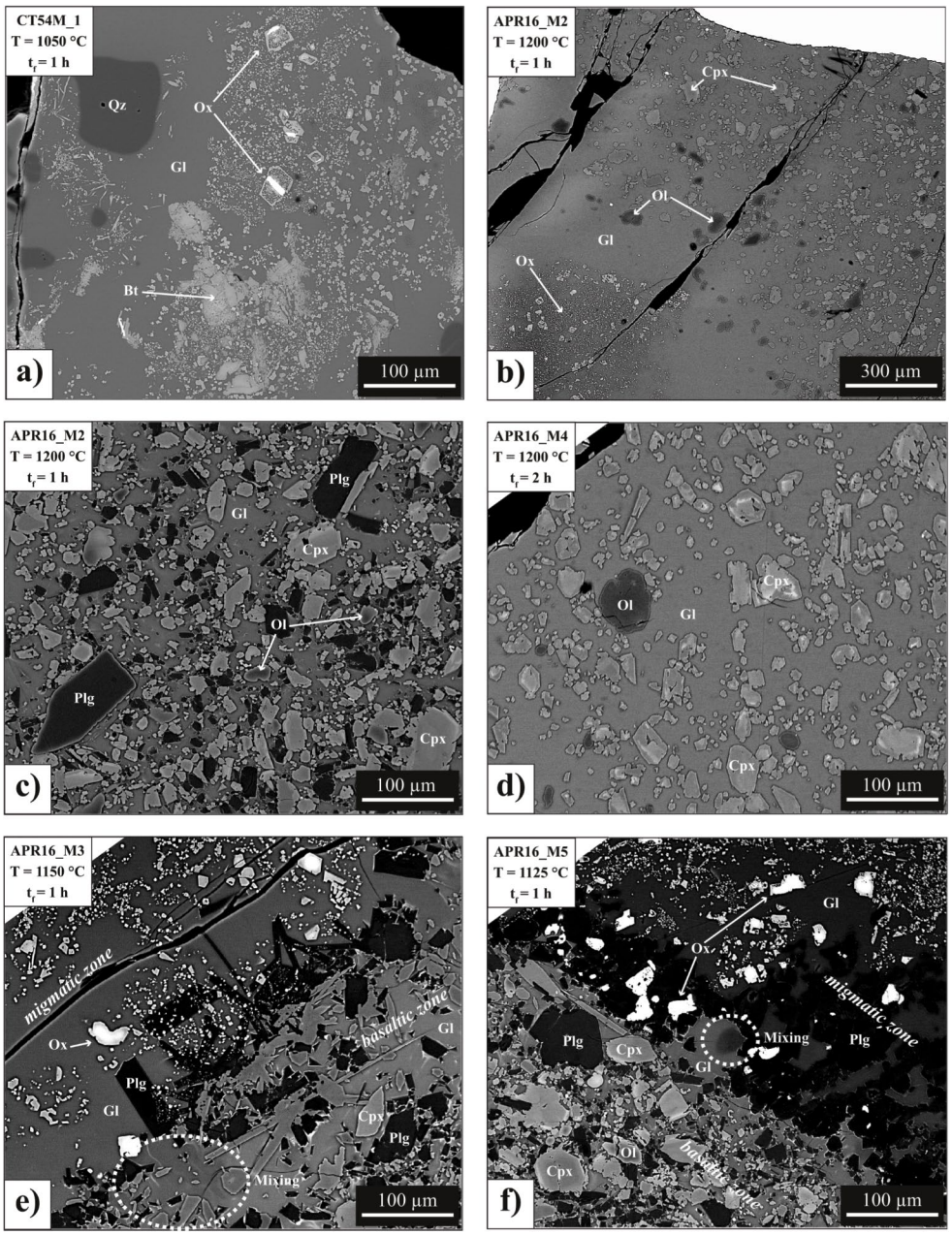

Fig. 5 Backscattered (BSE) images of run products obtained during isothermal experiments at 0.8 GPa, in the temperature range of 1050–1200 °C under natural water conditions. Details of the experimental conditions are reported in the upper part of each image. (a) Anhedral quartz surrounded by residual crystals of biotite and euhedral clustered oxides; (b) upper part of the capsule in which the melted migmatite characterized by the recrystallization of small, clustered hercynitic oxides is surrounded by clinopyroxene and olivine; (c) bottom zone of the capsule with a high amount of clinopyroxene, plagioclase and olivine; (d) mineral assemblage composed by clinopyroxene and olivine that appear uniformly distributed; (e) transition between the migmatitic and the *basaltic* zones (darker vs. lighter colour) signed by a high concentration of tabular crystals of labradoritic plagioclase and local injection of the migmatitic melt in the residual melt of the *basaltic zone* (dashed area); (f) local mixing (dashed area) between the migmatitic and the basaltic melts at the migmatite-basalt boundary. Abbreviation: Cpx: clinopyroxene; Plg: plagioclase; Ol: olivine; Ox: oxide; Qz: quartz; Bt: biotite; Gl: glass

melted (Fig. S2). Crystallized minerals appear uniformly distributed in the capsule and the estimated degree of crystallization is ~25 vol% (Fig. 2). As shown in Fig. 5d, the mineral assemblage is characterized by the absence of Plg and a slightly decrease of Cpx (~21 vol%) compared to the shortest run, although it remains the most abundant mineral phase. Here, unzoned clinopyroxenes and the rims of zoned crystals are augites ($Wo_{40-44}En_{48-51}Fs_{8-9}$), the core of the latter are diopsides ($Wo_{47-48}En_{42-43}Fs_{9-11}$). Ol ($Fo_{84-88}$; ~2 vol%) and oxides (~2 vol%) represent less abundant phases.

In the run performed at 1150 °C, migmatite in the inner part of the capsule is almost completely melted, except for some oxides, but it retains its original parallelepiped shape (Fig. S2). In the migmatitic melt, anhedral, rounded titanomagnetite relicts coexists with small subhedral equant, frequently clustered, new crystals of hercynite (< 10–15 µm). The transition between the migmatitic and the *basaltic* zones is signed by a high concentration of tabular, up to 50 µm sized crystals of labradoritic Plg (An_{51-54}) and, only in a very few points, it is possible to observe the local injection of the migmatitic melt in the residual melt of *basaltic zone* and mixing with it (Fig. 5e). In the *basaltic zone* (crystal fraction = ~53 vol%; Fig. 2) Cpx represents the first phase in abundance (~26 vol%). Also in this experiment Cpx is normally zoned showing a diopsidic core ($Wo_{45-49}En_{43-47}Fs_{8-9}$), and augitic rims ($Wo_{37-44}En_{46}$-$Fs_{9-17}$). In abundance Cpx is followed

by bytownitic Plg (An_{73-76}; ~19 vol%), Fo_{84-87} Ol (~7 vol%) and Cr-spinels (~1 vol%; Table 2).

At 1125 °C the fabric of experimental product is similar to that of run at 1150 °C: migmatite is almost fully melted and the shape of the pristine migmatite block is recognizable in the inner part of the capsule (Fig. S2). In this area the phase assemblage consists of migmatite-melt, relicts of Ti-magnetite and K-feld (Or_{73-74}) crystals and new hercynite microlites (< 25 µm in size) along with large, tabular to prismatic (up to ~100 µm in size) An_{48}-plagioclases present both within the area and at the transition between the migmatitic and the *basaltic zone*. Even in this case, local mixing between the migmatitic and the basaltic melts is evident at the migmatite-basalt boundary (Fig. 2f). The *basaltic zone* is characterized by a higher degree of crystallization (crystal fraction = ~59 vol%; Fig. 2) compared to higher temperature runs, and phase assemblage is composed, in order of abundance, of normally zoned and unzoned Cpx ($Wo_{38-48}En_{42-45}Fs_{10-17}$; ~32 vol%), bytownite Plg (An_{70-76}; ~18 vol%), Fo_{84-87} Ol (~7 vol%), and oxides (~2 vol%; Table 2) too small for reliable electron microprobe analysis.

Thermal gradient experiment

T-gradient experiment shows that mineral phases crystallized in the *basaltic zone* are similar to those formed in the constant temperature experiments (glass, Cpx, Ol, Plg and oxides; Table 2) but with proportions that vary according to temperature and chemical gradients. In particular, five zones characterized by peculiar textures have been recognised: four zones with different degree of crystallization and a holocrystalline zone near the partially melted migmatite (Fig. 6). In general, Cpx is the dominant mineral phase, homogeneously distributed along the *basaltic zone*. The size of these sub- to euhedral crystals ranges from 5 to 100 µm. Ol also displays sub- to euhedral habit with sizes varying from 5 to 100 µm. Plg, the second most abundant mineral phase, is smaller (5–50 µm) and exhibits sub- to euhedral tabular habit. Oxides instead, occur as traces characterized by a grain size of ≤ 10 µm making the acquisition of reliable EMP analyses difficult.

- *Zone 1*: slightly crystalline zone (crystal fraction = ~35 vol%). The extent of this zone is controlled by the furnace hot spot zone and it is about 0.5 mm in thickness (Fig. 6). We infer for this zone a temperature between 1250 °C and 1210 °C. Mineral assemblage is made up mainly of Cpx diopside ($Wo_{47-48}En_{43-44}Fs_{8-10}$; ~24 vol%), while bytownite Plg (An_{74}; ~6 vol%), Ol (Fo_{83}; ~3 vol%) and Cr-spinel (~2 vol%) are less abundant (Fig. 2).
- *Zone 2*: moderately crystalline zone (crystal fraction = ~40 vol%). The extent of this zone is limited to about 1 mm (Fig. 6) and the temperature ranges from 1210 °C to 1180 °C. Mineral phases are the same of *Zone 1* (Cpx + Plg + Ol + Ox) but there is a change in mineral proportions: Cpx ($Wo_{44-48}En_{43-47}Fs_{9-10}$; ~27 vol%) and Plg ($An_{76-78}$; ~10 vol%) amounts increases compared to Ol (Fo_{86-88}; ~2 vol%) and oxides (~1 vol%), that show a slight decrement (Fig. 2).
- *Zone 3*: considerably crystalline zone (crystal fraction = ~55 vol%). This zone, whose extent is limited to about 0.5 mm (Fig. 6), has a temperature range between 1180 °C and 1160 °C. Mineral assemblage is characterized by an increase of Plg (An_{69}; ~20 vol%), Ol (Fo_{87}; ~5 vol%) and oxide (~2 vol%) degree of crystallization compared to *Zone 2*, although Cpx ($Wo_{45-48}En_{43-45}Fs_{9-10}$; ~27 vol%) remains the most abundant mineral phase (Fig. 2).
- *Zone 4*: highly crystalline zone (crystal fraction = ~60 vol%). In this 0.5 mm thick zone (Fig. 6), whose temperature ranges between 1160 °C and 1140 °C, Cpx ($Wo_{46-49}En_{42-43}Fs_{9-11}$; ~28 vol%) represent the dominant phase followed by Plg (An_{72-76}; ~24 vol%), while Ol (Fo_{87}; ~6 vol%) and oxides (~2 vol%) remain less abundant (Fig. 2).
- *Zone 5*: holocrystalline zone. This zone spans from *Zone 4* up to the top of the capsule (10 mm thickness) and it is defined by rounded contacts with partially melted migmatite (Fig. 6). The temperature of this zone should be bracket by 1140 °C and 1000 °C. The crystal framework is composed in order of abundance of Plg (An_{71-78}; ~46 vol%), Cpx ($Wo_{45-49}En_{42-47}Fs_{8-9}$; ~39 vol%), Ol ($Fo_{84-88}$; ~11 vol%) and oxides (~4 vol%).
- *Zone M*: migmatite zone. The partially melted migmatite exhibits bevelled edges compared to its original parallelepiped shape (Fig. 6) and is characterized by absence of biotite, recrystallization of cordierite and increase of modal content Al-bearing phases, which contrasts with the migmatite previously described by Gaeta et al. (2018). The temperature estimated is between 1000 °C (i.e., the K-basalt solidus; Figs. 2) and 850 °C (i.e., the biotite-out; Vielzeuf and Schimdt 2001).

Composition of experimental glasses

Isothermal glasses

Compositions of residual glasses in the isothermal experiments are reported in Table S2. In the run conducted at 1200 °C with a dwell time of 1 h, glass composition is totally heterogeneous. In the *top zone*, it shifts from

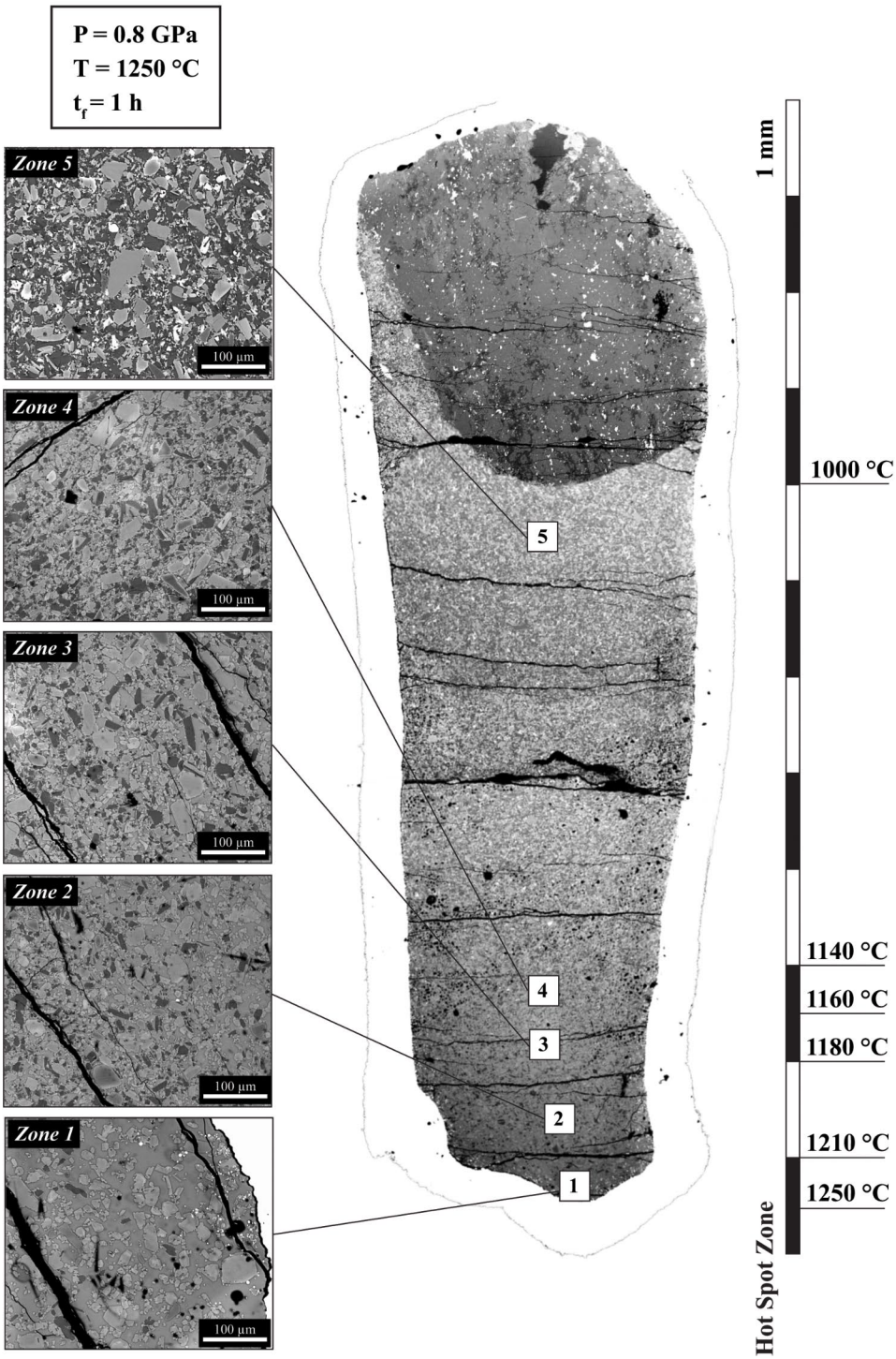

Fig. 6 Final product of the T-gradient experiment characterized by five zones: *Zone 1*) slightly crystalline zone (1250–1210 °C) made up of clinopyroxene, plagioclase, olivine and Cr-spinel; *Zone 2*) moderately crystalline zone (1210–1180 °C) composed by the same mineral phases of *Zone 1* but there is a change in mineral proportions; *Zone 3*) considerably crystalline zone (1180–1160 °C) characterized by an increase of plagioclase, olivine and oxides compared to *Zone 2*; *Zone 4*) highly crystalline zone (1160–1140 °C) in which clinopyroxene represent the dominant phase followed by plagioclase, while olivine and oxides remain less abundant; *Zone 5*) holocrystalline zone (1140–1000 °C) composed in order of abundance of plagioclase, clinopyroxene, olivine and oxides. The partially melted migmatite (1000–850 °C) exhibits bevelled edges compared to its original parallelepiped shape

K-trachybasalt towards shoshonite (point 1 and 1 M in Fig. 3) with decreasing distance with the melted migmatite. Moreover, it appears that moving to the melted migmatite, there is an increase of Al_2O_3 (from ~ 18.8 to ~ 20.7 wt%) and a decrement of MgO (from ~ 6.2 to ~ 3.8 wt%) and CaO (from ~ 8.7 to ~ 6.1 wt%) contents (point 1 and 1 M in Fig. 4). The *bottom zone*, that has a shoshonitic composition (point 2 in Fig. 3), reaches relatively high values of SiO_2 (~ 52.1 wt%), alkali (~ 6.9 wt%; Fig. 3), K_2O (~ 3.2 wt%) and Al_2O_3 (~ 19.2 wt%), and low contents of MgO (~ 4.6 wt%) and CaO (~ 6.8 wt%; Fig. 4). The run performed at 1200 °C with a dwell time of 2 h shows a more homogeneous K-trachybasalt composition, with a slightly increase of SiO_2 (up to ~ 50.8 wt%), MgO

(up to ~ 6.8 wt%) and CaO (up to ~ 8.9 wt%) and a slightly decrement of alkali (up to ~ 5.2 wt%), K_2O (up to ~ 2.5 wt%) and Al_2O_3 (up to ~ 18.4 wt%) compared to the glass 1 in the experiment at the same temperature but with a dwell time of 1 h (Figs. 3 and 4). In the run performed at 1150 °C, glass composition drives from shoshonite to trachyte showing a strong increase of SiO_2 (from ~ 52.1 to ~ 61.6 wt%), alkali (from ~ 6 to ~ 9.4 wt%; Fig. 3), K_2O (from ~ 3 to ~ 5.1 wt%) and Al_2O_3 (from ~ 18.3 to 19.5 wt%) and a decrease of MgO (from ~ 4.7 to ~ 1.5 wt%) and CaO (from ~ 6.6 to ~ 1.8 wt%) contents (Fig. 4), by passing from the *basaltic zone* to the migmatitic zone of the capsule. Glass derived from the mixing between the migmatitic and the basaltic melts shows intermediate contents of SiO_2 (~ 56.4 wt%), alkali (~ 7.8 wt%; Fig. 3), K_2O (~ 3.8 wt%), MgO (~ 3.2 wt%) and CaO (~ 4.2 wt%), coupled to high values of Al_2O_3 (~ 19.9 wt%) similar to those of the migmatitic glass (Fig. 4). In the run conducted at 1125 °C, glass shows shoshonitic to trachytic composition moving from the *basaltic zone* to the migmatitic zone (Fig. 3). In the *basaltic zone*, glass composition highlights an increment of SiO_2 (up to ~ 54.4 wt%), alkali (up to ~ 7.8 wt%; Fig. 3), K_2O (up to ~ 4.1 wt%), and Al_2O_3 (up to ~ 19.3 wt%), and a decrease of MgO (up to ~ 3.7 wt%) and CaO (up to ~ 5.2 wt%; Fig. 4), compared to the *basaltic zone* of the run performed at 1150 °C. The chemical composition of the migmatitic zone and the glass derived from the mixing between the migmatitic and the basaltic melts are comparable to those of the run performed at higher temperature (Fig. 4).

Thermal gradient glasses

Glass chemical composition varies as a function of degree of crystallization and phase assemblages from *Zone 1* at the bottom of the capsule (hot spot zone) to *Zone 4*, near the holocrystalline zone (Table S2). Glass composition ranges from shoshonite of *Zone 1* (where crystal fraction approaches ~ 35 vol% and T = 1250 °C) to phono-tephrite of *Zone 4* (Fig. 3). In particular, interstitial glass becomes phono-tephritic in composition when crystal fraction reaches ~ 55–60 vol%. The composition of glass is characterized by a slightly SiO_2 decrease passing from *Zone 1* (~ 50.9 wt%) to *Zone 4* (~ 50.1 wt%), coupled with an increase of alkali content (from ~ 6.8 to ~ 9.2 wt%) and K_2O (from ~ 2.6 to ~ 4 wt%; Fig. 4). Moreover, it appears that passing from *Zone 1* to *Zone 4*, the high degree of crystallization drives to a slightly decrease of Al_2O_3 (from ~ 19.5 to ~ 18.4 wt%) and strong decrease of CaO (from ~ 8.4 to ~ 5.7 wt%) and MgO (from ~ 6.1 to ~ 4.3 wt%) contents (Fig. 4).

Discussion

In a crustal context, petrological and geochemical evidence for anatectic melt extraction and restite formation is well documented in literature (e.g., Huppert and Sparks 1988; Mazzone 1989; Schnetger 1994; Patiñio Douce and Harris 1998; Otamendi and Patiñio Douce 2001; Droop et al. 2003; Gaeta et al. 2018). The dominant mechanism of anatexis in the continental crust is the incongruent melting of hydrous silicates (e.g., dehydration melting reaction of micas) to produce a hot, H_2O-undersaturated granitoid magma in conjunction with a less hydrous restitic assemblage (Brown and Fyfe 1970; Fyfe 1973; Clemens 1990; Stevens et al. 1997). The migration of granitoid magmas out of the deep crust leaves the lower crust in a dehydrated, restitic condition (Stevens et al. 1997). During melting events, SiO_2 and K_2O are preferentially partitioned in the anatectic melts, while restitic assemblages are enriched in Al_2O_3, TiO_2, FeO, MgO and CaO with respect to composition of protoliths (Patiñio Douce and Johnston 1990; Sinigoi et al. 1995; Droop et al. 2003). The phase relationships of melting of silica- and alumina-saturated crustal rocks show that K-feldspar, plagioclase, biotite, garnet, orthopyroxene, cordierite, corundum, magnetite, ilmenite and hercynite, can be important restitic phases during progressive anatexis of metasedimentary rocks (Patiñio Douce and Johnston 1990; Gaeta et al. 2018). After the first cycle of partial melting of the continental crust dominated by anatectic Si-rich melts, there may be a second cycle of crustal melting characterized by Al-rich melts. Our data support an experimental model for the reaction between restitic continental crust, represented by a leucosome depleted migmatite, and mantle-derived basaltic magma at the crustal-mantle boundary level.

Isothermal assimilation

The modal and compositional inhomogeneity and the abundant crystallization of Plg in the *bottom zone* of the open system experiment at 1200 °C and 1 h (Table 2) suggest that one hour is not enough time for the isenthalpic assimilation (Ghiorso and Kelemen 1987; Gaeta et al. 2021) of the SiO_2-, Al_2O_3-rich melt produced by the bulk melting of migmatite. The occurrence of heat gradient in the run at 1200 °C is caused by the large difference between the experimental temperature and the K-basalt crystallization and migmatite solidus temperature. Data on similar crustal rocks indicate the migmatite solidus at T < 950 °C (Vielzeuf and Schmidt 2001) in good agreement with the closed system experiment at 1050 °C characterized by about 65 wt% of migmatite melting. Consequently, in the open system at 1200 °C, the ΔT between the experimental temperature and migmatite solidus (hereafter $\Delta T_{exp\text{-}melt}$) is significantly higher

(> 250 °C) than the undercooling ($T_{liquidus}$-$T_{experiment}$ = ~ 80 °C; Table 2) of APR16 K-basalt (Perinelli et al. 2019; Bonechi et al. 2020). In the open system experiments at 1200 °C, the large $\Delta T_{exp\text{-}melt}$ favours the kinetic of partial melting respect to those of K-basalt crystallization. At the beginning (time = 0 h) of these experiments, the melting of migmatite in the *top zone* of the capsule (Fig. 1a) predates the K-basalt crystallization and the enthalpic gradient between the *top* and *bottom* zones of capsule starts. Actually, the migmatite melting is an endothermic process while the K-basalt crystallization is an exothermic process. The open-system experiment at 1200 °C and 1 h is isothermal but not isenthalpic and in the zone at lower heat content crystallized an amount of Plg and Ol larger respect to equilibrium conditions (Table 2; Fig. 2). The disequilibrium conditions are also indicated by the difference in water content between the top and bottom zones (Fig. S2 and Table S2) indicative of the presence of a H_2O gradient in 1 h experiment. Two hours are enough time to obtain the assimilation process in isothermal and isenthalpic conditions at 1200 °C. The glass in this experiment shows a composition that is not placed on the mixing line between K-basaltic and migmatitic compositions (Figs. 3 and 3), suggesting the origin of the differentiated melt from AFC process. The crystalline assemblage present in the open system experiment at 1200 °C and 2 h is different to that obtained in isothermal-closed conditions due to the lack of Plg and lower Cpx content. The change of phase relationships is due to a lowering of the liquidus temperature induced by an increase in the H_2O and K_2O contents caused by the bulk assimilation of migmatite that shows H_2O and K_2O contents of about 4 and 5 wt%, respectively (Table 1). The trachybasaltic melt obtained at 1200 °C, due to the decrease of Cpx and Plg crystallization, has higher contents of MgO and CaO than the trachybasaltic and shoshonitic melts obtained at similar temperatures (1220–1190 °C; Table 2; Figs. 3 and 4) in the closed-system. Noteworthy, the primitive (MgO = ~ 7 wt%) trachybasalt melt obtained with the experimental AFC at 1200 °C is characterized by the highest silica/alkali ratio that features also the melts obtained in the similar designed experiments at 1150 and 1125 °C. In the latter experiments, migmatite assimilation is not exclusively due to the AFC process because there are evidence of mingling and mixing. Actually, in the 1150 and 1125 °C isothermal open system experiments, the texture indicates a mingling process between the zone of melted migmatite and the zone of crystallized K-basalt and there are small melt polls with hybrid composition (Fig. 5e-f). In these experiments the activation energy of the melting and crystallization process are overcome simultaneously because the K-basalt undercooling and the $\Delta T_{exp\text{-}melt}$ of migmatite show close values. At time = 0 h of the 1150 and 1125 °C open-system experiments, K-basalt crystallization and migmatite melting begin and the two processes proceed almost independently for the contemporaneously formation of a rheological barrier. The boundary between the crystallized K-basalt and the melted migmatite is highlighted by the ghost image of the migmatite chip (Fig. S2) which remains approximately in the original position even if with different shape (rounded edges) and smaller dimensions. The rheological barrier originates from the different viscosity of K-basaltic and migmatitic melts and does not allow the bulk mixing between the two melts at time = 0 h. The chemical isolation of the migmatite zone is constrained by the glass composition, that is similar to the migmatite bulk composition (Table 1; Figs. 3 and 4), and by the occurrence of euhedral plagioclases (Fig. 5e-f) different in composition from those in the K-basaltic zone (Table S1). The rheological barrier works as semipermeable membrane that allows the diffusion of Si and Al from the migmatitic zone to the K-basaltic zone. In general, the shoshonitic melts obtained in the experimental AFC process at 1150 and 1125 °C together with the trachybasaltic one at 1200 °C form a differentiation trend characterized by a higher silica/alkali ratio compared to those obtained in closed-system experiments (Fig. 3). In particular, the melt in the 1125 °C open-system experiment has a higher Al/Si ratio than those of melts obtained in the closed system experiments (Fig. 4), in agreement with the assimilation of Al-rich crustal rocks that have been formed in a previous melting cycle. The isothermal open-system experiments suggest that the assimilation of Al-rich crustal rocks can also originate small amount of more differentiated magmas trough a mixing process coeval to the AFC process. Actually, the small melt polls latitic in composition in the open-system experiments at 1150 and 1125 °C falls on the mixing compositional line between the trachybasaltic melts obtained at 1200 °C and the migmatitic melt (Figs. 3, 4 and 5e-f).

Assimilation in T-gradient regime

Migmatitic zone in the thermal gradient experiment does not show glass in spite of a composition that at > 850 °C should have more than 10 vol% of melting (Vielzeuf and Schmidt 2001). This texture evidence, according to the peculiar composition of glasses in the 1–4 zones, indicates the migration of anatectic melt and confirms that also in T-gradient conditions the ACF process is experimentally simulated. However, the potassium content of glasses indicates difference between open system experiments at thermal gradient and isotherm conditions. Actually, low temperature zones of the T-gradient experiment have glasses with the highest alkali content. Moreover, the alkali enrichment is not correlated with the silica content that remain almost constant in the T-gradient experiment glasses. This liquid line of descent

is somewhat surprising because is obtained in a magmatic system open to the assimilation of Si-rich crust. The peculiar differentiation trend of glasses in the T-gradient experiment indicates that the assimilation component occurring at T < 1000 °C is different from those obtained at 1050 < T < 1200 °C in the isotherm experiments. The low MgO/K_2O and FeO/K_2O ratios of glass in the melting experiment at 1050 °C indicate a scarce contribution of biotite while the K-feld is the main reagent in the melting reaction. Actually, in the melting experiment at 1050 °C, the K-feld does not occur among the mineral phases and the composition of melt is close to the Qtz-Or binary eutectic of the haplogranite system at 1 GPa. Differently, the K-feld is relatively abundant in the migmatitic zone of the thermal gradient experiment. In this experiment, beyond the peculiar glass compositions, the phase relationships in the magmatic zones are different respect to those obtained in closed system experiments. At higher temperatures (1250–1225 °C, *Zone 1* in Fig. 6) and open-system conditions the mineral assemblage made up of Cpx + Plg + Ol + Ox is observed, although phase relationships in closed-system experiments at similar temperature and water content, predict only Cpx crystallization (Fig. 2). At lower temperatures, a large amount of crystals is observed in the alkaline basalt crystallised in open system conditions (Fig. 2). For example, a comparison between *Zone 2* assemblage and mineral phases crystallized in closed-system experiments at similar temperature (1190 °C; Fig. 2), shows a lower degree of crystallization of Plg in phase equilibria products (~3 wt%). At higher temperatures, the increment of Plg stability field in T-gradient conditions is correlated to the increase of alumina content in melt (Al_2O_3 = ~19.5 wt%) compared to closed system experiments (Al_2O_3 = ~17.5 wt%; Fig. 4). Overall, higher temperature glass of *Zone 1* shows the increment of K_2O (~2.6 wt%) content in comparison with closed system compositions (K_2O = ~1.9 wt%; Fig. 4). K_2O content increases in the melt from *Zone 1* to *Zone 4* because it is not incorporated into any crystallizing phase of the experimental AFC process that is controlled by the Ol + Cpx + Plg + Ox crystallization in a system open to the migmatite assimilation. In particular, the assimilation component in the T-gradient experiment is represented almost exclusively by the biotite breakdown in the migmatite that causes the increase of Al, Mg, Fe, Ti and K activities in the system. The high Al activity causes the strong increase of Plg degree of crystallization, from ~6 vol% (*Zone 1*) up to ~24 vol% (*Zone 4*; Fig. 2; Table 2) that, in turn, drives to a marked decrease of CaO content in the residual melt (Fig. 4). This experimental result is in accord with Bowen's prediction (1922) that the assimilation of aluminous sediment in basaltic magma would increase the modal proportion of plagioclase. The decrement of CaO content, as well as MgO content, is also influenced by Cpx, whose abundant crystallization (~28 vol% in *Zone 4*) is also controlled by the high Ti activity. In the T-gradient experiment, the breakdown of Ti-rich, restitic biotite causes, indeed, the crystallization of clinopyroxenes richer in TiO_2 content (0.8–1.7 wt%) compared to those crystallized in closed-system experiments (0.6–0.9 wt%; Perinelli et al. 2019). The high amount of Ol in *Zone 4*, as well as of oxide in *Zone 5*, are explainable by AFC process in which the assimilation component causes the increase of Mg and Fe and the decrease of Si activities. These chemical features are compatible with the breakdown of migmatite biotite occurring in the quartz and K-feldspar stability field.

There is a high degree of mismatch between results of the AFC simulated in gradient conditions and MELTS calculations on K-basalt (calculation details in Table S3 and in Supplementary materials). In detail, while the paragenesis of experimental results at 1250 °C (*Zone 1*) is Gl + Cpx + Plg + Ol + Ox, that computed by MELTS is Gl + Cpx, according to closed system experiments. Analogously, the paragenesis of open-system experiment results at 1210 °C (*Zone 2*), 1180 °C (*Zone 3*) and 1160 °C (*Zone 4*) is Gl + Cpx + Plg + Ol + Ox, whereas that predicted by MELTS modelling is Gl + Cpx + Plg + Ox; MELTS yields Ol crystallization exclusively at T = 1130 °C, at those run conditions. Additionally, MELTS calculations show SiO_2 increase in the residual melt according to closed-system experiments, in contrast with silica decrement evidenced passing from *Zone 1* to *Zone 4* of the open-system experiment. It appears that in MELTS modelling the dominant crystallization of Cpx drives to an increase of Al_2O_3 content in residual melt, until Plg crystallizes; this behaviour disagrees with the marked decrease of Al_2O_3 shown in the open-system experiment.

Deep magma storage in melt depleted continental crust

Our experimental results allow us to discuss for the first time the interaction between primitive basaltic magmas and continental crust previously interested by melting processes and how this interaction affects Al_2O_3 and alkali enrichment (Fig. 7). In particular, our results can support petrological and geochemical studies addressed to reconstruct the differentiation processes at the origin of the igneous rock types of Campi Flegrei volcanic district (from silica-saturated to slightly silica-undersaturated, potassic compositions) and in general the complex evolution of the Campanian magma systems (Peccerillo 2017 and references therein). This magmatism has been characterized by an early calc-alkaline volcanic cycle that may have promoted a first episode of deep crustal melting (Fig. 8a). On the other hand, anatectic magmas has been recognized in the older Quaternary volcanoes

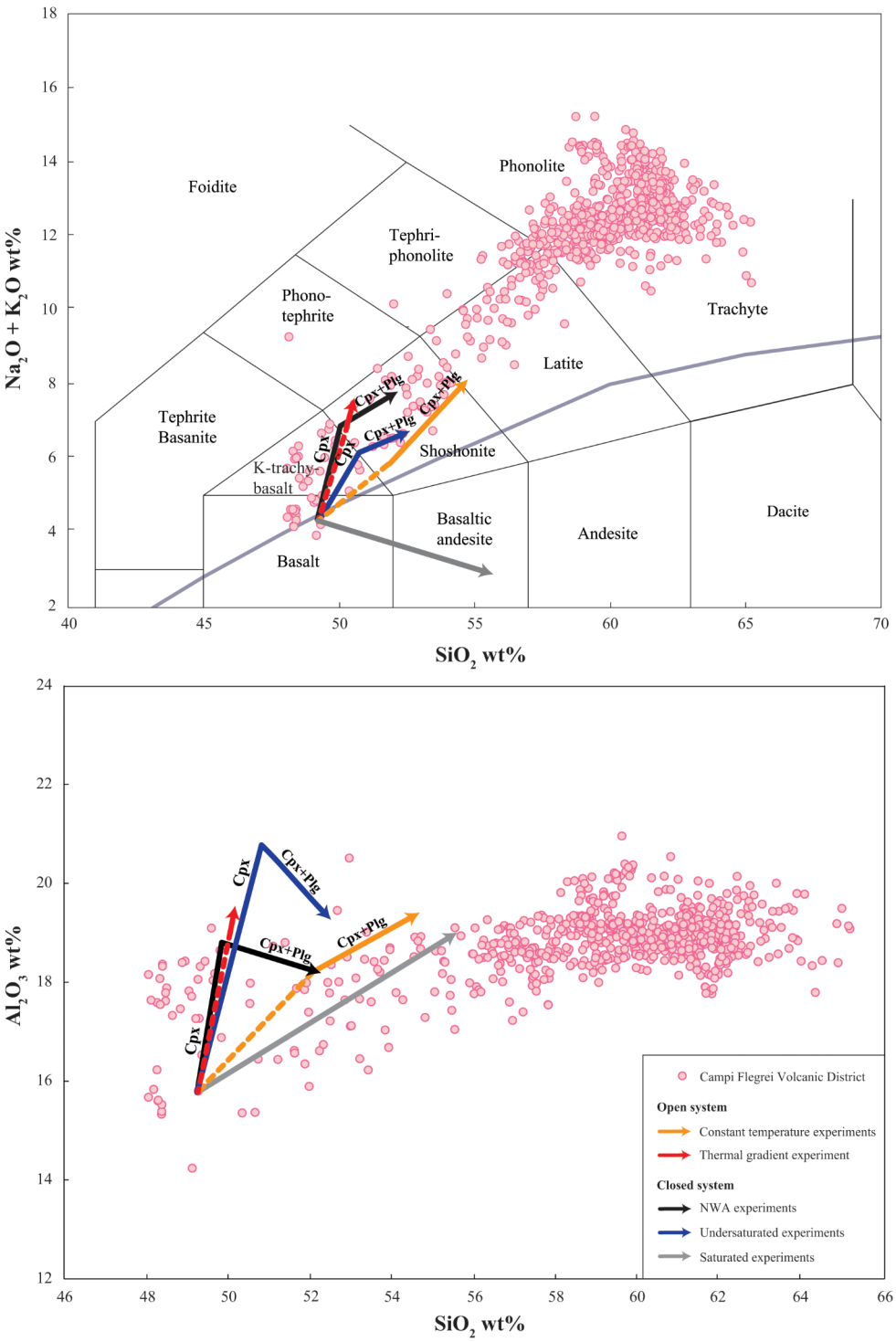

Fig. 7 Total alkali vs. silica (TAS; Le Maitre et al. 2002) and Al_2O_3 vs. SiO_2 diagrams showing the compositional evolution of residual melts in relation to the crystallized minerals of isothermal and T-gradient runs in open system and of phase equilibria experiments (no water added, undersaturated, saturated) in closed system. Literature data of Campi Flegrei Volcanic District products are from GEOROC database (http://georoc.mpch-mainz.gwdg.de/georoc/Start.asp). Abbreviation: Cpx: clinopyroxene; Plg: plagioclase; NWA: no water addition to the starting materials

of central Italy of comparable age to those of Campanian calc-alkaline rocks (Conticelli et al. 2013; Peccerillo 2017).

Many geochemical and thermodynamic models (e.g., Pappalardo et al. 2002; Di Renzo et al. 2007, 2011; Fowler et al. 2007; D'Antonio 2011; D'Antonio et al. 2013; Brown et al. 2014; Gebauer et al. 2014; Mazzeo et al. 2014; Melluso et al. 2014; Fedele et al. 2016; Forni et al. 2016; Iovine et al. 2017; Di Salvo et al. 2020; Bonechi et al. 2023) indicate that geochemical and isotopic variations of magmas of Campi Flegrei volcanic district (CFVD) can be explained by fractional crystallization as the dominant mechanisms, associated with assimilation events possibly occurred in both deeper and shallower reservoirs or only during the magma stagnation at shallow depth. Actually, previous

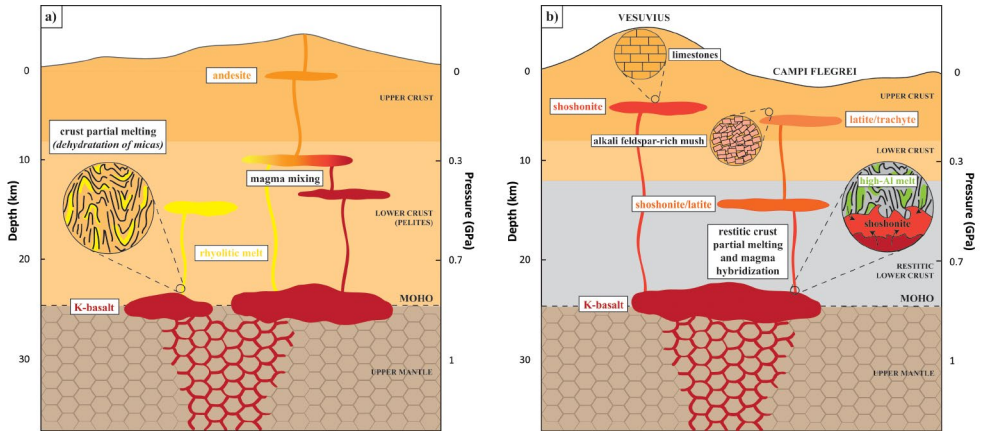

Fig. 8 (a) Schematic model of lower crust partial melting dominated by anatectic Si-rich melts associated to an early calc-alkaline volcanic cycle; (b) schematic model of restitic lower crust (Hercynian basement) assimilation dominated by high-Al melts during which primitive K-basalt magmas differentiated toward shoshonitic-latitic composition. This scenario could explain the genesis of the parental magma relative to both CFVD and Vesuvius magmatic systems that, at shallow depth, interacts with alkali feldspar rich-rock/mush (CFVD system) and with Meso-Cenozoic limestones and dolostones (Vesuvius system)

experimental studies on near-primary K-basaltic compositions recognized as possible parental magmas of the recent (< 50 ka) volcanic products of the Campania Province (e.g., Mazzeo et al. 2014), do not completely satisfy a scenario of magmas differentiation related merely to fractionation processes in a closed-system. Indeed, crystallization at equilibrium in a closed system of a K-basalt of composition such as that of APR16, in undersaturated conditions, produces a differentiation trend characterized by a decrease in Al_2O_3 content in the residual melts as plagioclase begins to crystallize (Fig. 7). Such trends are different from that observed in the compositions of CFVD products where a general positive correlation between Al_2O_3 and SiO_2 is observed, particularly for Campi Flegrei volcanics. For a closed-system, a similar correlation was obtained through H_2O-saturated experiments, conditions under which the plagioclase crystallization is suppressed. However, the residual glasses produced in these experiments are variously depleted in alkalis due to the preferential partitioning of sodium and potassium in the hydrous fluid coexisting with H_2O-saturated melt (Fig. 7; Perinelli et al. 2019). This resulted in the convergence of the composition of the latter towards the subalkaline field in contrast with the positive correlation between alkalis and SiO_2 typical of CFVD volcanics.

In the scenario of assimilation events occurred in both deeper and shallower reservoirs, geochemical models suggest that magmas generated in the upper mantle were probably modified in a lower crust storage zone at depths of > 8 km (Zollo et al. 2008) by mixing with partially melted Hercynian basement (Fig. 8b). Energy-constrained assimilation + fractional crystallization modeling (EC-AFC; Spera and Bohrson 2001) constraints the deep history of batches of mantle-derived magma in not more than ~ 7% of assimilation of granodioritic rocks from continental crust (e.g., D'Antonio et al. 2013; Gebauer et al. 2014; Iovine et al. 2017) during which basalt-trachybasalt magmas differentiated toward shoshonitic-latitic composition (Fig. 8b). Then, this magma evolved at shallow depth mainly by fractional crystallization coupled with mingling/mixing processes between distinct magmas and also by interaction with the feldspar-rich crystal mush zones accumulated in the CFVD plumbing system by fractional crystallization of magmas that fed older eruptions (Pappalardo et al. 2002; Di Renzo et al. 2007; Renzo et al. 2011; Fowler et al. 2007; Arienzo et al. 2009; D'Antonio 2011; D'Antonio et al. 2013; Brown et al. 2014; Gebauer et al. 2014; Fedele et al. 2016; Forni et al. 2016; Iovine et al. 2017). Concerning the CFVD magma storage phase in the deep zones, experiments in systems open to the assimilation of an aluminium-enriched, continental crust give rise to parental shoshonitic to latitic magmas that do not show depletion in Al_2O_3 despite being in equilibrium with plagioclase (Fig. 7). Moreover, it should be noted that the produced experimentally glasses have higher Al_2O_3 contents than those used as the parent magma by Fowler et al. (2007) and Brown et al. (2014) to model the evolutionary line of the CF and Ischia magmas, respectively, and that both modelling indicate the assimilation in the shallow reservoirs of alkali feldspar rich-rock / mush (Fig. 8b), a necessary step to extend the liquid line of descent of a shoshonite/latite to the natural, high SiO_2 and Al_2O_3, evolved trachytes and phonolites.

The geochemical characteristics acquired in the high-pressure assimilation process could imply the need for less assimilation of feldspathic rocks at shallow depths. In addition, the composition obtained in gradient experiments in which assimilation of the almost exclusive biotite component was achieved for the first time, resulting in a shoshonitic composition in which an enrichment in alkali coupled

with a constancy of SiO_2 content is observed (Fig. 7), could represent the parental magma relative to both CFVD and Vesuvius magmatic systems that at shallow depth: the first interacted more or less with a crystalline igneous rocks of monzonitic-syenitic (sensu lato) composition (Fig. 8b; e.g., D'Antonio 2011; Brown et al. 2014), the second interacted possibly with the basement composed of Meso- Cenozoic limestones and dolostones (Fig. 8b; e.g., Savelli 1968; Del Moro et al. 2001; Pappalardo et al. 2004; Di Renzo et al. 2007; Dallai et al. 2011).

Conclusions

In the present study we aim to investigate the interaction between restitic continental crust and primitive K-basaltic magma at the crustal-mantle boundary level. Continental crust was previously interested by melting processes dominated by anatectic Si-rich melts, generating Al-rich restitic rocks. According to the assimilation of Al-rich crustal rocks, open-system isothermal experiments evidence that trachybasaltic to shoshonitic melts obtained in the experimental AFC process form a differentiation trend characterized by a positive correlation between Al_2O_3 and SiO_2, even when plagioclase begins to crystallize, and by a higher silica/alkali ratio compared to closed system experiments conducted at equilibrium conditions using a primitive K-basalt as starting material. In addition to the AFC process, open system experiments at 1150 and 1125 °C show evidence of a coeval mixing process that originates more evolved latitic melts. Although the texture of the T-gradient experiment confirms that even in this case the AFC process is well simulated, the K_2O and SiO_2 contents of residual glasses (shoshonitic to phono-tephritic composition) highlights differences with isothermal experiment trend. Indeed, low temperature zones of the T-gradient experiment exhibit glasses with the highest alkali content, whereas the silica content remains almost constant. The cause of these differences can be attributed to the assimilation component that in the T-gradient experiment is represented almost exclusively by the biotite breakdown in the migmatite occurring in the quartz and K-feldspar stability field, leading to an increase in Al, Mg, Fe, Ti, and K activities and a decrease of Si activity in the system. The shoshonitic composition obtained in the T-gradient experiment could potentially reproduce the parental magma for both the CFVD and Vesuvius magmatic systems. According to this scenario, magmas originated in the upper mantle were modified within the lower crust, where they mixed with partially melted Hercynian basement rocks. During this process, basalt-trachybasalt magmas differentiated towards shoshonitic-latitic compositions. Subsequently, this magma evolved at shallow depths by interaction with feldspar-rich crystal mush zones accumulated within the CFVD plumbing system and with the basement composed of Meso- Cenozoic limestones and dolostones of the Vesuvius magmatic system.

Supplementary Information The online version contains supplementary material available at https://doi.org/10.1007/s00410-024-02127-y.

Acknowledgements We are grateful to associate editor Gordon Moore for the manuscript handling. We also thank two anonymous reviewers for their constructive comments, which have contributed to improving the manuscript. C. Perinelli's research is supported by funds of the PNRR PE3: RETURN projects - multi-Risk sciEnce for resilicnT commUnities undeR a changiNg climate area tematica 3 "Rischi ambientali, naturali e antropici" Spoke 3, the Italian Ministry of Education, University and Research (MIUR). M. Racek (Institute of Petrology and Structural Geology, Charles University of Prague) is thanked for assistance during EMPA analytical sessions. We thank T. Ruspandini (Department of Earth Sciences, Sapienza University of Rome) for assistance during SEM analytical sessions.

Funding Open access funding provided by Università degli Studi di Roma La Sapienza within the CRUI-CARE Agreement.

Data availability All the available data and figures supporting our findings are given in the text and supplementary files.

References

Abramoff MD, Magalhães PJ, Ram SJ (2004) Image Processing with ImageJ. Biophotonics Int 11:36–42

Arienzo I, Civetta L, Heumann A, Wörner G, Orsi G (2009) Isotopic evidence for open system processes within the Campania Ignimbrite (Campi Flegrei - Italy) magma chamber. Bull Volcanol 71:285–300. https://doi.org/10.1007/s00445-008-0223-0

Asimow PD, Ghiorso MS (1998) Algorithmic modifications extending MELTS to calculate subsolidus phase relations. Am Mineral 83:1127–1132. https://doi.org/10.2138/am-1998-9-1022

Bonechi B, Perinelli C, Gaeta M (2020) Clinopyroxene growth rates at high pressure: constraints on magma recharge of the deep reservoir of the Campi Flegrei Volcanic District (south Italy). Bull Volcanol 82:5. https://doi.org/10.1007/s00445-019-1342-5

Bonechi B, Fabbrizio A, Perinelli C, Gaeta M (2023) Experimental investigation of trace element partitioning between amphibole and alkali basaltic melt: towards a more general partitioning model with implications for amphibole fractionation at deep crustal

levels. Am Mineral 108:1678–1691. https://doi.org/10.2138/am-2022-8536
Borisova AY, Bohrson WA, Spera FJ (2021) Magma-Rock and Magma-Mush interactions as fundamental processes of magmatic differentiation. Front Earth Sci 9:665588. https://doi.org/10.3389/feart.2021.665588
Bowen NL (1922) The behavior of inclusions in igneous magmas. J Geol 30:513–570
Bowen NL (1928) The evolution of the igneous rocks. Princeton University Press, Princeton, NJ
Brown GC, Fyfe WS (1970) The production of granitic melts during ultrametamorphism. Contrib Mineral Petrol 28:310–318. https://doi.org/10.1007/BF00388953
Brown RJ, Civetta L, Arienzo I, D'Antonio M, Moretti R, Orsi G, Tomlinson EL, Albert PG, Menzies MA (2014) Geochemical and isotopic insights into the assembly, evolution and disruption of a magmatic plumbing system before and after a cataclysmic caldera-collapse eruption at Ischia volcano (Italy). Contrib Mineral Petrol 168:1–23. https://doi.org/10.1007/s00410-014-1035-1
Clemens JD (1990) The granulite-granite connexion. Granulites and crustal evolution. Springer Netherlands, Dordrecht
Conticelli S, Avanzinelli R, Poli G, Braschi E, Giordano G (2013) Shift from lamproite-like to leucititic rocks: Sr–Nd–Pb isotope data from the Monte Cimino volcanic complex vs. the Vico stratovolcano, Central Italy. Chem Geol 353:246–266
Couch S, Sparks RSJ, Carroll MR (2003) The kinetics of degassing-induced crystallization at Soufriere Hills Volcano, Montserrat. J Petrol 44:1477–1502. https://doi.org/10.1093/petrology/44.8.1477
D'Antonio M (2011) Lithology of the basement underlying the Campi Flegrei caldera: volcanological and petrological constraints. J Volcanol Geotherm Res 200:91–98. https://doi.org/10.1016/j.jvolgeores.2010.12.006
D'Antonio M, Tonarini S, Arienzo I, Civetta L, Dallai L, Moretti R, Orsi G, Andria M, Trecalli A (2013) Mantle and crustal processes in the magmatism of the Campania region: inferences from mineralogy, geochemistry, and Sr-Nd-O isotopes of young hybrid volcanics of the Ischia island (South Italy). Contrib Mineral Petrol 165:1173–1194. https://doi.org/10.1007/s00410-013-0853-x
Dallai L, Cioni R, Boschi C, D'Oriano C (2011) Carbonate-derived CO_2 purging magma at depth: influence on the eruptive activity of Somma-Vesuvius, Italy. Earth Plan Sci Lett 310:84–95
Dallai L, Bianchini G, Avanzinelli R, Deloule E, Natali C, Gaeta M, Cavallo A, Conticelli S (2022) Quartz-bearing rhyolitic melts in the Earth's mantle. Nat Commun 13:7765. https://doi.org/10.1038/s41467-022-35382-3
Del Moro A, Fulignati P, Marianelli P, Sbrana A (2001) Magma contamination by direct wall rock interaction: constraints from xenoliths from the walls of a carbonate-hosted magma chamber (Vesuvius 1944 eruption). J Volcanol Geotherm Res 112:15–24. https://doi.org/10.1016/S0377-0273(01)00231-1
DePaolo DJ (1981) Trace element and isotopic effects of combined wall rock assimilation and fractional crystallization. Earth Planet Sci Lett 53:189–202. https://doi.org/10.1016/0012-821X(81)90153-9
Di Renzo V, Di Vito MA, Arienzo I, Carandente A, Civetta L, D'Antonio M, Giordano F, Orsi G, Tonarini S (2007) Magmatic history of Somma-Vesuvius on the basis of new geochemical and isotopic data from a deep borehole (Camaldoli della Torre). J Petrol 48:753–784. https://doi.org/10.1093/petrology/egl081
Di Renzo V, Arienzo I, Civetta L, D'Antonio M, Tonarini S, Di Vito MA, Orsi G (2011) The magmatic feeding system of the Campi Flegrei caldera: architecture and temporal evolution. Chem Geol 281:227–241. https://doi.org/10.1016/j.chemgeo.2010.12.010
Di Rocco T, Freda C, Gaeta M, Mollo S, Dallai L (2012) Magma chambers emplaced in carbonate substrate: petrogenesis of skarn and cumulate rocks and implications for CO_2 degassing in volcanic areas. J Petrol 53:2307–2332. https://doi.org/10.1093/petrology/egs051
Di Salvo S, Avanzinelli R, Isaia R, Zanetti A, Druitt T, Francalanci L (2020) Crystal-mush reactivation by magma recharge: evidence from the Campanian Ignimbrite activity, Campi Flegrei volcanic field, Italy. Lithos 376:105780. https://doi.org/10.1016/j.lithos.2020.105780
Droop GTR, Clemens JD, Dalrympl DJ (2003) Processes and conditions during contact anatexis, melt escape and restite formation: the Huntly Gabbro Complex, NE Scotland. J Petrol 44:995–1029. https://doi.org/10.1093/petrology/44.6.995
Fedele L, Scarpati C, Sparice D, Perrotta A, Laiena F (2016) A chemostratigraphic study of the Campanian ignimbrite eruption (Campi Flegrei, Italy): insights on magma chamber withdrawal and deposit accumulation as revealed by compositionally zoned stratigraphic and facies framework. J Volcanol Geotherm Res 324:105–117. https://doi.org/10.1016/j.jvolgeores.2016.05.019
Forni F, Bachman O, Mollo S, De Astis G, Gelmand SG, Ellisa BS (2016) The origin of a zoned ignimbrite: insights into the Campanian Ignimbrite magma chamber (Campi Flegrei, Italy). Earth Planet Sci Lett 449:259–271. https://doi.org/10.1016/j.epsl.2016.06.003
Fowler SJ, Spera FJ, Bohrson WA, Belkin HE, De Vivo B (2007) Phase equilibria con- straints on the chemical and physical evolution of the Campanian Ignimbrite. J Petrol 48:459–493. https://doi.org/10.1093/petrology/egl068
Fyfe WS (1973) A discussion on the evolution of the precambrian crust-the granulite facies, partial melting and the archaean crust. Philosophical Trans Royal Soc Lond Ser Math Physl Sci 273:457–461. https://doi.org/10.1098/rsta.1973.0011
Gaeta M, Di Rocco T, Freda C (2009) Carbonate assimilation in open magmatic systems: the role of melt-bearing skarns and cumulate-forming processes. J Petrol 50:361–385. https://doi.org/10.1093/petrology/egp002
Gaeta M, Giuliani A, Di Rocco T, Tecchiato V, Perinelli C, Kamenetsky VS (2018) Isotopic disequilibrium in migmatitic hornfels of the Gennargentu Igneous Complex (Sardinia, Italy) records the formation of low $^{87}Sr/^{86}Sr$ melts from a mica-rich source. J Petrol 59:1309–1328. https://doi.org/10.1093/petrology/egy062
Gaeta M, Bonechi B, Marra F, Perinelli C (2021) Uncommon K-foiditic magmas: the case study of Tufo Del Palatino (Colli Albani Volcanic District, Italy). Lithos 396:106239. https://doi.org/10.1016/j.lithos.2021.106239
Gebauer SK, Schmitt AK, Pappalardo L, Stockli DF, Lovera OM (2014) Crystallization and eruption ages of Breccia Museo (Campi Flegrei Caldera, Italy) plutonic clasts and their relation to the campanian ignimbrite. Contrib Mineral Petrol 167:1–18. https://doi.org/10.1007/s00410-013-0953-7
Ghiorso MS, Kelemen PB (1987) Evaluating reaction stoichiometry in magmatic systems evolving undergeneralized thermodynamic constraints; examples comparing isothermal and isenthalpic assimilation. In: Mysen BO (ed) Magmatic Processes: Physiochemical Principles. A Volume in Honour of Hatten S. Yoder Jr, Geochemical Society, Special Publications 1, pp 319–336
Ghiorso MS, Sack RO (1995) Chemical mass-transfer in magmatic processes. A revised and internally consistent thermodynamic model for the interpolation of liquid-solid equilibria in magmatic systems at elevated temperatures and pressures. Contrib Min Petrol 119:197–212. https://doi.org/10.1007/BF00307281
Huppert HE, Sparks RSJ (1988) The generation of granitic magmas by intrusion of basalt into continental crust. J Petrol 29:599–624. https://doi.org/10.1093/petrology/29.3.599
Iovine RS, Mazzeo FC, Arienzo I, D'Antonio M, Wörner G, Civetta L, Pastore Z, Orsi G (2017) Source and magmatic evolution inferred from geochemical and Sr-O-isotope data on hybrid lavas of Arso, the last eruption at Ischia island (Italy; 1302 AD).

J Volcanol Geotherm Res 331:1–15. https://doi.org/10.1016/j.jvolgeores.2016.08.008

Irvine TN, Baragar WRA (1971) A guide to the chemical classification of the common volcanic rocks. Can J Earth Sci 8:523–548. https://doi.org/10.1139/e71-055

Knuever M, Sulpizio R, Mele D, Costa A (2023) Magma-rock interactions: a review of their influence on magma rising processes with emphasis on short-timescale assimilation of carbonate rocks. Geol Soc Spec Publ 520:101–120. https://doi.org/10.1144/SP520-2021-17

Le Maitre RW, Streckeisen A, Zanettin B, Le Bas MJ, Bonin B, Bateman P, Bellieni G, Dudek A, Efremova S, Keller J, Lameyre J, Sabine PA, Schmid R, Sørensen H, Woolley AR, Schmid R (2002) Igneous rocks. A classification and glossary of terms: recommendations of the International Union of Geological Sciences Subcommission on the Systematics of Igneous Rocks. Cambridge Univ

Masotta M, Freda C, Gaeta M (2012) Origin of crystal-poor, differentiated magmas: insights from thermal gradient experiments. Contr Mineral Petrol 163:49–65

Mazzeo FC, D'Antonio M, Arienzo I, Aulinas M, Di Renzo V, Gimeno D (2014) Subduction-related enrichment of the Neapolitan volcanoes (Southern Italy) mantle source: new constraints on the characteristics of the slab-derived components. Chem Geol 386:165–183. https://doi.org/10.1016/j.chemgeo.2014.08.014

Mazzone P (1989) Peraluminous xenoliths in kimberlite: metamorphosed restites produced by partial melting of pelites. Geochim Cosmochim Acta 53:1551–1561. https://doi.org/10.1016/0016-7037(89)90237-8

McLeod CL, Davidson JP, Nowell GM, De Silva SL (2012) Disequilibrium melting during crustal anatexis and implications for modeling open magmatic systems. Geology 40:435–438. https://doi.org/10.1130/G33000.1

Melluso L, Morra V, Guarino V, De Gennaro R, Franciosi L, Grifa C (2014) The crystallization of shoshonitic to peralkaline trachyphonolitic magmas in a H_2O-Cl-F-rich environment at Ischia (Italy), with implications for the feeder system of the Campania Plain volcanoes. Lithos 210:242–259. https://doi.org/10.1016/j.lithos.2014.10.002

Morabito S, Petrosino P, Milia A, Sprovieri M, Tamburrino S (2014) A multidisciplinary approach for reconstructing the stratigraphic framework of the last 40 ka in a bathyal area of the eastern Tyrrhenian Sea. Glob Planet Change 123:121–138. https://doi.org/10.1016/j.gloplacha.2014.10.005

Morimoto N (1988) Die Nomenklatur Von Pyroxenen. Mineral Petrol 39:55–76. https://doi.org/10.1007/BF01226262

Otamendi JE, Patiño Douce AE (2001) Partial melting of aluminous metagreywackes in the Northern Sierra De Comechingones, Central Argentina. J Petrol 42:1751–1772. https://doi.org/10.1093/petrology/42.9.1751

Pappalardo L, Piochi M, D'Antonio M, Civetta L, Petrini R (2002) Evidence for multi- stage magmatic evolution during the past 60 kyr at Campi Flegrei (Italy) deduced from Sr, nd and pb isotope data. J Petrol 43:1415–1434. https://doi.org/10.1093/petrology/43.8.1415

Pappalardo L, Piochi M, Mastrolorenzo G (2004) The 3550 year BP-1944 AD magma-plumbing system of Somma-Vesuvius: constraints on its behaviour and present state through a review of Sr-Nd isotope data. Ann Geophys. http://hdl.handle.net/2122/845

Patiño Douce AE, Harris N (1998) Experimental constraints on himalayan anatexis. J Petrol 39:689–710. https://doi.org/10.1093/petroj/39.4.689

Patiño Douce AE, Humphreys ED, Johnston AD (1990) Anatexis and metamorphism in tectonically thickened continental crust exemplified by the Sevier hinterland, western North America. Earth Planet Sci Lett 97:290–315. https://doi.org/10.1016/0012-821X(90)90048-3

Peccerillo A Association internationale de volcanologie et de chimie de l'intérieur de la Terre (2017) Cenozoic volcanism in the Tyrrhenian Sea region. New York, NY, USA: Springer

Perinelli C, Orlando A, Conte AM, Armienti P, Borrini D, Faccini B, Misiti V (2008) Metasomatism induced by alkaline magma on upper mantle of the Northern Victoria Land (Antarctica): an experimental approach. In Coltorti M, Grégoire M (eds) Mantle metasomatism in intraplate and suprasubduction settings. Geological Society, London, Special Publications 293;197–221

Perinelli C, Gaeta M, Bonechi B, Granati SF, Freda C, D'Antonio M, Stagno V, Sicola S, Romano C (2019) Effect of water on the phase relations of primitive K-basalts: implications for high-pressure differentiation in the Phlegraean Volcanic District magmatic system. Lithos 342:530–541. https://doi.org/10.1016/j.lithos.2019.05.032

Savelli C (1968) The problem of rock assimilation by Somma-Vesuvius magmas, II, compositions of sedimentary rocks and carbonate ejecta from Vesuvius area. Contrib Mineral Petrol 18:43–64. https://doi.org/10.1007/BF00371985

Schnetger B (1994) Partial melting during the evolution of the amphibolite-to granulite-facies gneisses of the Ivrea Zone, northern Italy. Chem Geol 113:71–101. https://doi.org/10.1016/0009-2541(94)90006-X

Sinigoi S, Quick JE, Mayer A, Demarchi G (1995) Density-controlled assimilation of underplated crust, Ivrea-Verbano Zone, Italy. Earth Planet Sci Lett 129:183–191. https://doi.org/10.1016/0012-821X(94)00230-V

Spera FJ, Bohrson WA (2001) Energy-constrained open-system magmatic processes I: general model and energy-constrained assimilation and fractional crystallization (EC-AFC) formulation. J Petrol 42:999–1018. https://doi.org/10.1093/petrology/42.5.999

Stevens G, Clemens JD, Droop GT (1997) Melt production during granulite-facies anatexis: experimental data from primitive metasedimentary protoliths. Contrib Mineral Petrol 128:352–370. https://doi.org/10.1007/s004100050314

Vielzeuf D, Schmidt MW (2001) Melting relations in hydrous systems revisited: application to metapelites, metagreywackes and metabasalts. Contrib Mineral Petrol 141:251. https://doi.org/10.1007/s004100100237

Zollo A, Maercklin N, Vassallo M, Dello Iacono D, Virieux J, Gasparini P (2008) Seismic reflections reveal a massive melt layer feeding Campi Flegrei caldera. Geophys Res Lett 35:L12306. https://doi.org/10.1029/2008GL034242